PLL Position and Speed Observer With Integrated Current Observer for Sensorless PMSM Drives

Cristian Lascu and Gheorghe-Daniel Andreescu, *Senior Member, IEEE*

***Abstract*—In this article, a phase-locked loop (PLL) rotor position and speed observer, including an integrated decoupled stator current observer, is proposed for wide-speed-range sensorless control of permanent magnet synchronous motor (PMSM) drives. This new PLL scheme consists of two interconnected observers: 1) a second-order PLL position observer using the direct current error as correction term and 2) a third-order extended Luenberger speed observer, based on the mechanical model of the drive, using the quadrature current error as the correction term. The estimated speed is just an unrefined reference for the position integrator, and it is further corrected by the PLL. The current observer is a subsystem integrated as a PLL phase detector. Key relations between the current errors and the position and speed errors are proven, and a practical two-step observer design method is presented. A method for real-time identification of the stator resistance at low speeds and of the permanent magnet flux at high speeds is proposed, using the current errors in the current reference frame. Experimental results for a 0.5-kW surface-mounted PMSM drive confirm the effectiveness, excellent dynamic performance, and robustness of the new PLL observer. Stable motor and generator operation at 15 r/min (0.01 p.u.) with ramp and step speed reversals, high-speed operation, and stator resistance adaptation is shown.**

***Index Terms*—Permanent magnet motor drives, phase-locked loops (PLLs), sensorless control, state observers, variable-speed drives.**

I. Introduction

THE PERMANENT magnet synchronous motors (PMSMs) are used in variable-speed drives due to their high power and torque density, high efficiency, wide speed range, and small size. Position and speed transducers for drives are unreliable and noise sensitive and increase the size, weight, and cost. To avoid these problems, sensorless control methods based on observers, using only current and voltage transducers, have been developed [1], [2]. The technology is mature, but reliable operation of ac drives at very low speeds remains a major challenge, since the electromotive force (EMF) is low.

Sensorless control methods for PMSM drives are divided into two main classes [1], [2]: i) fundamental excitation model-based methods, used at medium–high speeds [3]–[16], and ii) high-frequency signal injection (HFSI) methods, used mostly at standstill and at low speeds [17]–[23]. Hybrid methods combine (i) and (ii) to achieve a wide speed range [24]–[26].

The *HFSI methods* use voltage signals with frequencies of 0.5–1 kHz and small amplitudes to detect the rotor position and speed. The following strategies are used:

1) sinusoidal HFSI [17]–[19] that extracts the rotor speed from the stator current harmonics using filtering techniques;
2) square-wave HFSI [20], [21], where the position error is proportional with quadrature current variation over a sampling period. It removes low-pass filters, increasing the bandwidth;
3) low-frequency (50-Hz) pulse voltage injection [22], where the harmonic currents are extracted without filters, but enhanced vector-tracking observers and notch filters are used;
4) fundamental pulsewidth modulation (PWM) excitation based on the stator current derivative in each PWM cycle, without explicit injection [23].

All HFSI methods are stable at zero and low speeds, but they only work for motors with saliency and produce additional losses, noise, and vibrations.

The methods based on *fundamental excitation modeling* avoid the problems related to signal injection and estimate the rotor position and speed using the fundamental waves of the stator currents and voltages. These schemes are practical for speeds larger than several percent of the rated speed. For low-speed operation, the stator voltage and the EMF are very small, and the stator current is low for unloaded operation. Therefore, most observers are sensitive to voltage distortions caused by inverters, nonlinearities and unmodeled dynamics, and motor parameter variations. The state observers employed for estimation in PMSM drives are as follows:

1) EMF-based methods that estimate the stator current and the extended EMF vectors using disturbance observers,

Manuscript received April 30, 2019; revised August 13, 2019, December 4, 2019, and January 7, 2020; accepted January 12, 2020. Date of publication February 13, 2020; date of current version March 4, 2020. *(Corresponding author: Cristian Lascu.)*

Cristian Lascu is with the Department of Electrical Engineering, University Politehnica of Timisoara, 300006 Timisoara, Romania (e-mail: cristian.lascu@et.upt.ro).

Gheorghe-Daniel Andreescu is with the Department of Automation and Applied Informatics, University Politehnica of Timisoara, 300006 Timisoara, Romania (e-mail: daniel.andreescu@aut.upt.ro).

Color versions of one or more of the figures in this article are available online at https://ieeexplore.ieee.org.

Digital Object Identifier 10.1109/TIE.2020.2972434

either linear [3], [4] or sliding mode [5]. The speed and position are calculated from the EMF or using the observation errors;

2) speed-adaptive Luenberger observers, either full order or reduced order, which estimate the stator current and flux vectors [6]–[8]. The speed is estimated using a proportional–integral (PI) adaptation mechanism fed by the current error. Stable operation at 30 r/min (0.02 p.u.) with step load, using a reduced-order observer with stator resistance adaptation, is reported in [8]. Zero-speed operation is possible when it is combined with HFSI [6];
3) the hypothetical rotor position approach proposed by Matsui [9] uses the current and voltage models in a hypothetical rotor reference frame to evaluate the position and speed. The lowest speed reported is 100 r/min (0.08 p.u.) at full load. A new extended observer based on the same idea, using detailed EMF errors between models, appears in [10];
4) model reference adaptive observers (MRAO), where the voltage model is the reference model, the current model is the adaptive model, and the estimated position is the adaptive parameter [11]. The smallest speed reported is 0.02 p.u.;
5) active flux observers proposed in [12] use either a full-order observer or an MRAO with an adaptive voltage model [13] to estimate the active flux vector. The rotor position is estimated as the position of the active flux. Low speed of 2 r/min (0.02 p.u.) at half rated torque is reported in [13];
6) phase-locked loop (PLL) position and speed observers [14]–[16]. A PLL estimator for reluctance machines using the direct and quadrature current models is described in [14]. A novel finite-position-set PLL is used to estimate the EMF and speed for a surface-mounted PMSM generator in [15]. Significant reduction of oscillations, robustness against parameter variations, and a minimum speed of 0.024 p.u. with half-load are reported.

This article proposes a new fifth-order PLL position and speed observer based on the fundamental excitation model, for wide-speed-range sensorless control of PMSM drives. This scheme integrates a decoupled stator current observer that plays the role of a phase detector (PD) for the PLL. The original contributions of this article consist of: 1) key relationships between the current errors and the position and speed errors; 2) a new observer topology using two interconnected observers with independent corrections: a) second-order PLL position observer with the direct current error as correction term and b) third-order extended Luenberger speed observer with the quadrature current error as the correction term; and 3) sensitivity analysis and real-time adaptation mechanisms for stator resistance and permanent magnet (PM) flux. Experimental results confirm the effectiveness and robustness of the new observer for wide-speed-range operation. Stable motor and generator operation at 15 r/min (0.01 p.u.) with stator resistance estimation proves the excellent static and dynamic performance.

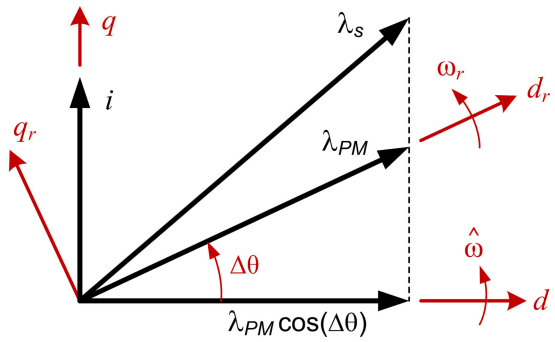

Fig. 1. Real (d_r q_r) and estimated (d q) reference frames for PMSM.

II. PMSM Model

In order to facilitate the design of a generic rotor position observer for PMSMs, two reference frames are considered, as shown Fig. 1: 1) the real rotor reference frame (d_r q_r) with the direct axis d_r oriented along the PM flux $\lambda_{\rm PM}$, which has the rotor position θ_r and rotates with the rotor speed ω_r, and 2) an estimated rotor reference frame (d q), which has an estimated rotor position $\hat{\theta}$ and rotates with an estimated rotor speed $\hat{\omega}$. The rotor position and speed errors are defined as $\Delta\theta = \theta_r - \hat{\theta}$ and $\Delta\omega = \omega_r - \hat{\omega}$, respectively. As the real frame position is always unknown, all following considerations and equations are related to the estimated reference frame.

The PMSM dynamic model in the (d q) estimated rotor frame is

$$u_s = R_s i + \frac{d}{dt}\lambda_s + j\hat{\omega}\lambda_s \tag{1}$$

$$\lambda_s = \lambda_{\rm PM} e^{j\Delta\theta} + L_d i_d + jL_q i_q \tag{2}$$

where $u_s = u_{sd} + ju_{sq}$ and $i = i_d + ji_q$ are the stator voltage and current vectors, respectively, $\lambda_s = \lambda_d + j\lambda_q$ is the stator flux vector, $\lambda_{\rm PM}$ is the PM flux, L_d and L_q are the d- and q-axis inductances, respectively, and R_s is the stator resistance. For small $\Delta\theta$, the estimated inductances are $\hat{L}_d(\Delta\theta) \cong L_d$ and $\hat{L}_q(\Delta\theta) \cong L_q$ [9], [10].

Substituting the stator flux from (2) into (1), the PMSM model in the (d q) *estimated rotor reference frame* is obtained, where the stator currents are state variables

$$L_d\frac{d}{dt}i_d = u_{sd} - R_s i_d + \hat{\omega}L_q i_q + \omega_r\lambda_{\rm PM}\sin(\Delta\theta) \tag{3}$$

$$L_q\frac{d}{dt}i_q = u_{sq} - R_s i_q - \hat{\omega}L_d i_d - \omega_r\lambda_{\rm PM}\cos(\Delta\theta). \tag{4}$$

This PMSM model is nonlinear, cross-coupled, with time-variable parameters, and it depends on both the real speed $\omega_r = \hat{\omega} + \Delta\omega$ and the estimated speed $\hat{\omega}$. The EMF terms are functions of the real speed and contain valuable information on the rotor position error $\Delta\theta$.

A simple second-order mechanical model of a drive is

$$\frac{J}{p}\frac{d}{dt}\omega_r = T_e - T_L, \quad \frac{d}{dt}T_L = 0 \tag{5}$$

$$T_e = 1.5p\left(\lambda_{\rm PM} i_q + (L_d - L_q)\, i_d i_q\right) \tag{6}$$

where T_e is the electromagnetic torque, T_L is the load torque, J is the rotor inertia, and p is the number of pole pairs.

III. Current Observer

An observer is a real-time model of a process or system, which is driven by the available inputs and outputs of the real system, and delivers the system state vector estimation. An observer contains two main parts: 1) a system model, which could be an approximate, simplified, or reduced-order model, and 2) a feedback compensator that corrects the model using the error between the real system output and the observer output. An observer can be designed for a system if and only if that system is completely observable [28].

A simplified PMSM model based on (3) and (4) is used to design a *decoupled current observer* in the (d q) estimated rotor frame. The observer is described by

$$L_d \frac{d}{dt}\hat{i}_d = u_{sd} - R_s\hat{i}_d + \hat{\omega}L_q i_q + K_d\Delta i_d \tag{7}$$

$$L_q \frac{d}{dt}\hat{i}_q = u_{sq} - R_s\hat{i}_q - \hat{\omega}L_d i_d - \hat{\omega}\lambda_{\mathrm{PM}} + K_q\Delta i_q \tag{8}$$

where $\Delta i_d = i_d - \hat{i}_d$ and $\Delta i_q = i_q - \hat{i}_q$ are the current errors, and K_d and K_q are positive gains.

The correction terms $K_d\Delta i_d$ and $K_q\Delta i_q$ approximate the disturbances, namely, the EMF terms in (3) and (4) that contain the position error $\Delta\theta$ between the real and estimated frames. Note that the cross-coupling terms $\hat{\omega}L_q i_q$ and $\hat{\omega}L_d i_d$ use the measured currents (i_d, i_q), same as in the real model (3), (4), while the EMF term $\hat{\omega}\lambda_{\mathrm{PM}}$ uses the estimated speed $\hat{\omega}$ instead of the real speed ω_r.

The observer state is the estimated current vector $\hat{i} = \hat{i}_d + j\hat{i}_q$, while the stator voltage u_s, actual stator current i, and the estimated speed $\hat{\omega}$ are inputs.

The current error dynamic model (9), (10) was obtained by subtracting the decoupled current observer model (7), (8) from the PMSM model (3), (4). Note that it contains relevant information related to the position and speed errors

$$L_d \frac{d}{dt}\Delta i_d = -\left(R_s + K_d\right)\Delta i_d + \omega_r\lambda_{\mathrm{PM}}\sin\left(\Delta\theta\right) \tag{9}$$

$$L_q \frac{d}{dt}\Delta i_q = -\left(R_s + K_q\right)\Delta i_q - \lambda_{\mathrm{PM}}\left(\omega_r\cos\left(\Delta\theta\right) - \hat{\omega}\right). \tag{10}$$

The current error model is decoupled and has the structure of two low-pass filters with the time constants $L_d/(R_s + K_d)$ and $L_q/(R_s + K_q)$. These time constants can be made arbitrarily small by increasing the gains. Considering only the steady-state operation of these filters and small position errors, the current errors are proportional with the EMF differences, i.e., the last terms in (9) and (10)

$$\Delta i_d \cong \omega_r\lambda_{\mathrm{PM}}\Delta\theta/\left(R_s + K_d\right) \tag{11}$$

$$\Delta i_q \cong -\lambda_{\mathrm{PM}}\Delta\omega/\left(R_s + K_q\right). \tag{12}$$

Relations (11) and (12) are true for small position errors and provide key dependencies between the current errors and the rotor position and speed errors. A position observer acting on this information must implement a compensator that drives the estimated position toward the real one. This is precisely what a PLL system does.

IV. Rotor Position and Speed Observers

Equations (11) and (12) prove that, for small position errors, the direct current error is proportional with the position error multiplied by the rotor speed, while the quadrature current error is proportional with the speed error. These attributes are used to design two interconnected observers with two distinct corrections: 1) a rotor position observer using the direct current error Δi_d as correction, and 2) a rotor speed observer using the quadrature current error Δi_q as correction. Both errors are evaluated from the current observer (7), (8).

A *PLL observer* is employed to estimate the rotor position, and an *extended Luenberger observer* is used to estimate the rotor speed. A generic block diagram of the proposed position and the speed observer is shown in Fig. 2. This schematic has the topology of a PLL system, where the direct current observer (Obs i_d) plays the role of a PD with $\Delta i_d \approx \omega_r\Delta\theta$, while the position integrator plays the role of a voltage-controlled oscillator (VCO). The quadrature current observer (Obs i_q) delivers $\Delta i_q \approx -\Delta\omega$ as input for the speed observer (Obs ω), which produces the speed estimation $\hat{\omega}$ that acts as an unrefined reference for the position observer. An alternative estimated speed $\hat{\omega}_1$ is obtained at the input of the position integrator. This estimated speed has zero error in the steady-state operation.

A. PLL Position Observer

A PLL is a closed-loop system that contains a PD, a loop filter, and a VCO. The designer has complete freedom to decide the structure of this system, as long as an appropriately designed controller (loop filter) drives the phase error to zero.

The PD for the new PLL observer is formed by the direct current observer (7) together with the $\alpha\beta$-to-dq frame transformations, which produces a current error proportional with the phase error $\Delta i_d \approx \omega\Delta\theta$. The oscillator is an integrator that estimates the rotor position, followed by the computation of $\sin(\hat{\theta})$ and $\cos(\hat{\theta})$. The loop filter is a simple proportional controller with speed adaptive gain.

The second-order *direct current and position observer* is

$$L_d \frac{d}{dt}\hat{i}_d = u_{sd} - R_s\hat{i}_d + \hat{\omega}L_q i_q + K_d\Delta i_d \tag{13}$$

$$\frac{d}{dt}\hat{\theta} = \hat{\omega} + k_\theta\ \mathrm{sign}\ (\hat{\omega})\,\Delta i_d = \hat{\omega}_1 \tag{14}$$

where $k_\theta = K_\theta/|\hat{\omega}|$ is a positive speed-adaptive gain.

The observer states are $\hat{i}_d$ and $\hat{\theta}$; the inputs are u_{sd}, i_q, and $\hat{\omega}$. The correction is Δi_d, proportional with the position error $\Delta i_d \approx \hat{\omega}\Delta\theta$. As mentioned, the cross-coupling term in (13) uses the measured current that effectively decouples the d and q current equations and provides a simpler implementation and design.

The estimated speed $\hat{\omega}$ can be regarded as a raw speed reference that is further corrected by the PLL. As the d-current error is proportional with the speed, an ideal correction for speed in (14)

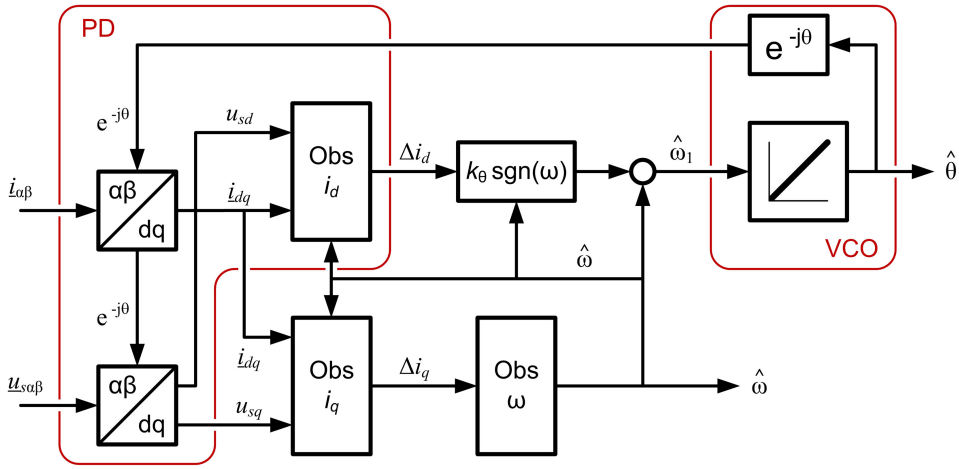

Fig. 2. PLL position and speed observer with an integrated current observer as a PD.

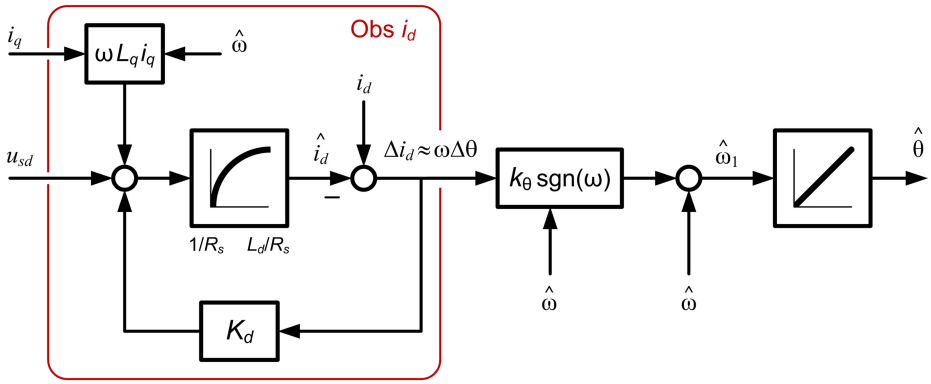

Fig. 3. PLL position estimator using the *d*-axis current observer as the PD for $\Delta i_d \approx \omega\Delta\theta$.

must be speed adaptive, i.e., $k_\theta = K_\theta/|\hat{\omega}|$ with K_θ constant. To avoid very large gains at low speeds, a simple gain scheduling strategy for k_θ is used: large constant values at low speeds and small values at high speeds.

A detailed diagram of the PLL rotor position observer is shown in Fig. 3. This stands for the upper half of Fig. 2, less the frame transformations. The implementation of the direct current observer (13) includes a first-order low-pass filter with the gain $K = 1/R_s$ and the time constant $T = L_d/R_s$.

B. Extended Speed Observer

A third-order *extended Luenberger observer* is designed to estimate the rotor speed. Similarly to PLLs, the model and the topology of an observer can be freely selected by the designer, as long as it implements a correction mechanism that drives the estimation error to zero [1], [28]. The *speed observer* (15)–(18) contains the quadrature current observer described by (8) and a second-order speed and load torque observer based on the mechanical model of the drive (5), (6)

$$L_q \frac{d}{dt}\hat{i}_q = u_{sq} - R_s\hat{i}_q - \hat{\omega}L_d i_d - \hat{\omega}\lambda_{\mathrm{PM}} + K_q\Delta i_q \qquad (15)$$

$$\frac{d}{dt}\hat{\omega} = \left(T_e - \hat{T}_L\right)\frac{p}{J} + K_\omega\Delta i_q \qquad (16)$$

$$\frac{d}{dt}\hat{T}_L = K_T\Delta i_q \qquad (17)$$

$$T_e = 1.5p\left(\lambda_{\mathrm{PM}} i_q + (L_d - L_q)\, i_d i_q\right) \qquad (18)$$

where K_q, K_ω, and K_T are the observer gains.

The observer states are $\hat{i}_q$, $\hat{\omega}$, and $\hat{T}_L$; the inputs are u_q, i_d, and T_e. The correction is Δi_q, proportional with the speed error $\Delta i_q \approx -\Delta\omega$. The electromagnetic torque T_e (18) is computed using the measured current. Fig. 4 shows a block diagram of the quadrature current observer followed by the speed and load torque observer. The implementation of the quadrature current observer (15) includes a first-order low-pass filter with the gain $K = 1/R_s$ and the time constant $T = L_q/R_s$.

C. Observer Gain Design

The complete PLL observer shown in Fig. 2 is a fifth-order system that contains two frequency-separated subsystems. The third-order position, speed, and load torque observer, formed by (14), (16), and (17), estimates the slowly changing mechanical

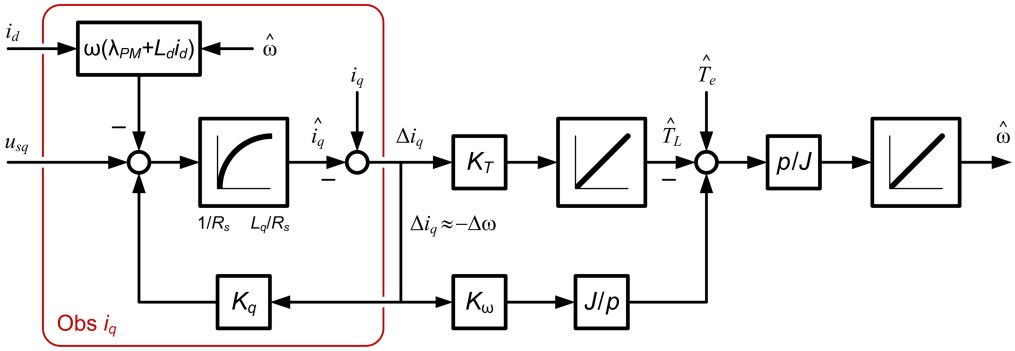

Fig. 4. Speed and load torque estimators using the q-axis current observer for $\Delta i_q \approx -\Delta\omega$.

variables, while the second-order current observer, formed by (13) and (15), estimates the fast stator currents. Therefore, the gains are separately selected for the fast and slow dynamic subsystems by using a pole placement design.

1) Current Observer Gains: Consider the current error dynamic model (9), (10) of the current observer (7), (8). Assuming zero position error and zero speed error, the simplified current error dynamics is

$$L_d \frac{d}{dt}\Delta i_d = -\left(R_s + K_d\right)\Delta i_d \tag{19}$$

$$L_q \frac{d}{dt}\Delta i_q = -\left(R_s + K_q\right)\Delta i_q. \tag{20}$$

The observer poles are $p_d = -(R_s + K_d)/L_d$ and $p_q = -(R_s + K_q)/L_q$. The design for current gains K_d and K_q is given by selecting two negative poles (p_d, p_q) for fast response

$$K_d = -\left(L_d p_d + R_s\right), \quad K_q = -\left(L_q p_q + R_s\right). \tag{21}$$

For example, for the experimental drive with surface PMs $(L_d \cong L_q)$, by selecting $p_d = p_q$ for a bandwidth of 500 Hz, we obtain equal gains $K_d = K_q = K_{dq} = 300$ V/A.

2) Speed and Position Observer Gains: To design the gains for the mechanical subsystem (14), (16), and (17), the current errors are substituted by their steady-state approximations from (11) and (12). Now, this subsystem contains only mechanical quantities, and its error dynamic is

$$\frac{d}{dt}\begin{bmatrix}\Delta\theta\\ \Delta\omega\\ \Delta T_L\end{bmatrix} = \begin{bmatrix}-K_\theta k_s & 1 & 0\\ 0 & K_\omega k_s & -k_j\\ 0 & K_T k_s & 0\end{bmatrix}\begin{bmatrix}\Delta\theta\\ \Delta\omega\\ \Delta T_L\end{bmatrix} \tag{22}$$

where $k_s = \lambda_{\rm PM}/(R_s + K_{dq})$ and $k_j = p/J$ are parameters.

The observer is stable if three real negative poles (p_1, p_2, and p_3) are selected for (22). Then, the gains can be solved from the characteristic equation of (22), equivalent to the system (23)

$$\begin{aligned}\left(K_\omega - K_\theta\right)k_s &= p_1 + p_2 + p_3\\ \left(K_T k_j - K_\theta K_\omega k_s\right)k_s &= p_1p_2 + p_2p_3 + p_3p_1\\ -K_T K_\theta k_j {k_s}^2 &= p_1p_2p_3.\end{aligned} \tag{23}$$

The analytical solution of (23) is quite involved, and it is convenient to solve for the gains numerically, starting with some desired poles. As the gain for position estimation in (14) is speed dependent, we set its maximum value at low speeds as $k_{\theta\max} = K_\theta$, which is valid for a speed of 1 rad/s. At high speeds, we set $k_\theta = K_\theta/300$.

V. Stator Resistance and PM Flux Estimation

A. Sensitivity Analysis for Parameter Uncertainty

The key equations (11) and (12) assume identical parameters between the current observer and the PMSM model. In reality, all parameters are variables: the PM flux $\lambda_{\rm PM}$ decreases with rotor temperature, the stator resistance R_s increases with stator temperature, and L_d and L_q inductances decrease with saturation.

To analyze the sensitivity of position and speed estimations to parameter variations, let us assume that the observer uses inaccurate parameters. The parameter deviations are defined as $\Delta R_s = R_s - \hat{R}_s$, $\Delta\lambda_{\rm PM} = \lambda_{\rm PM} - \hat{\lambda}_{\rm PM}$, and $\Delta L_{d,q} = L_{d,q} - \hat{L}_{d,q}$. Then, the current error dynamic model is evaluated as the difference between the PMSM model (3), (4) and the current observer model (7), (8). For steady-state operation, the current errors Δi_d and Δi_q are negligible, being the correction terms in (7) and (8). The rotor position and speed errors are dependent on the rotor speed ω and PMSM parameter deviations, as follows:

$$\Delta\theta \cong \left(-\Delta L_q i_q + \Delta R_s i_d/\omega\right)/\left(\lambda_{\rm PM} + \Delta\lambda_{\rm PM}\right) \tag{24}$$

$$\Delta\omega \cong -\left(\omega(\Delta\lambda_{\rm PM} + \Delta L_d i_d) + \Delta R_s i_q\right)/\lambda_{\rm PM}. \tag{25}$$

In the steady state, the estimated rotor speed $\hat{\omega}_1$ at the input of the position integrator in Fig. 2 is constant, with zero error. Therefore, only the rotor position error $\Delta\theta$ is considered as critical for accurate sensorless control. At low speeds, $\Delta\theta$ is mostly affected by the stator resistance error $\Delta R_s i_d/[\omega(\lambda_{\rm PM} + \Delta\lambda_{\rm PM})]$, while at high speeds, the small error in quadrature inductance $-\Delta L_q i_q/(\lambda_{\rm PM} + \Delta\lambda_{\rm PM})$ prevails.

For the experimental PMSM described in Section VI, let consider the following parameter variations:$\Delta R_s = 10\%R_s$, $\Delta\lambda_{\rm PM} = -5\%\lambda_{\rm PM}$, and $\Delta L_{d,q} = -10\%L_{d,q}$, and maximum values for currents $i_d = 0.5$ A and $i_q = 1.5$ A. In this case, the *position error* (24) is $\Delta\theta \in (0.018,\ 0.88/\omega)$ rad. The 10% error of the L_q inductance produces a small position error $\Delta\theta = 1.03^\circ$ (0.018 rad), and the inductance estimation will not be further considered. For an electrical speed of 3 rad/s (0.01 p.u.) and for 10% R_s error, the position error is large,

$\Delta\theta = 17°$; thus, the stator resistance estimation must be used at low speeds. The PM flux variation affects the position error (24) to a lesser degree, and its estimation is optional. With the same parameter variations as before, the *speed error* (25) is $\Delta\omega = \omega_r - \hat{\omega} \in (-2.5,\ 5.5\%\ \omega)$ rad/s. At high speeds, $\Delta\omega$ is large, mostly determined by $\Delta\lambda_{\rm PM}(\Delta\omega = 5\%\omega)$, with little effect produced by ΔL_d ($\Delta\omega = 0.5\%\ \omega$). At low speeds, $\Delta\omega$ is small, mostly determined by ΔR_s ($\Delta\omega = -2.5$ rad/s). The speed error affects only the unrefined estimated speed $\hat{\omega}$, while the estimated speed $\hat{\omega}_1$ has zero error in steady-state operation.

In conclusion, in order to obtain an accurate convergence for both position and speed estimation, the real-time stator resistance adaptation is required at low speeds, while the PM flux estimation is optional at high speeds.

B. Stator Resistance and PM Flux Estimations

The stator resistance changes with the temperature and its error have a substantial impact at low-speed operation (24), (25).

A novel stator resistance estimator is proposed employing the *stator current reference frame*. In its own reference frame, denoted by ($x\,y$), the actual stator current has only the direct component $\underline{i}_s = i_x = |\underline{i}_s|$. Due to modeling and parameter errors, the estimated current $\hat{\underline{i}}_{xy} = \hat{i}_x + j\hat{i}_y$ has a nonzero quadrature component $\hat{i}_y$. Let us define by $\hat{\theta}_i$ the angle of estimated current vector, and θ_i the angle of the real current. Using the frame transformation from $\alpha\beta$ to xy, the quadrature current is

$$\hat{\underline{i}}_y = \left(\hat{i}_\beta \cos\hat{\theta}_i - \hat{i}_\alpha \sin\hat{\theta}_i\right) = \left(i_\alpha\hat{i}_\beta - i_\beta\hat{i}_\alpha\right) \Big/ |\underline{i}_s|\,. \quad (26)$$

If the parameter estimation loop is convergent, then $\hat{\theta}_i \cong \theta_i$, and thus, $\cos\hat{\theta}_i \cong i_\alpha/|\underline{i}_s|$ and $\sin\hat{\theta}_i \cong i_\beta/|\underline{i}_s|$ in (26). The estimated currents ($\hat{i}_\alpha,\ \hat{i}_\beta$) are obtained from the current observer (7), (8) using the dq-to-$\alpha\beta$ transformation.

The proposed stator resistance estimator (27) drives to zero the $\hat{i}_y$ component, that is the numerator $(i_\alpha\hat{i}_\beta - i_\beta\hat{i}_\alpha)$ of (26), using an integral compensator

$$\hat{R}_s = R_{s0} - K_{Rs}\frac{1}{s}\left(i_\alpha\hat{i}_\beta - i_\beta\hat{i}_\alpha\right)\cdot \text{sign}\,(\hat{\omega}) \quad (27)$$

where R_{s0} is the cold stator resistance (constant), K_{Rs} is a small positive gain, and s is the Laplace operator. The rotor speed sign is taken into account to achieve correct estimation at both positive and negative speeds. The estimated stator resistance (27) includes the actual stator resistance plus the equivalent ON-state resistance of the inverter insulated-gate bipolar transistors (IGBTs) and diodes. The inverter dead time is compensated in the controller.

An equation that uses a similar correction term was found for the PM flux estimation in real time

$$\hat{\lambda}_{\rm PM} = \lambda_{\rm PM0} - K_{\rm PM}\frac{1}{s}\left(i_\alpha\hat{i}_\beta - i_\beta\hat{i}_\alpha\right)\text{sign}\,(T_e) \quad (28)$$

where $K_{\rm PM}$ is a positive gain and λ_{PM0} is the rated PM flux.

However, the PM flux and the stator resistance cannot be simultaneously identified by using the same correction (26).

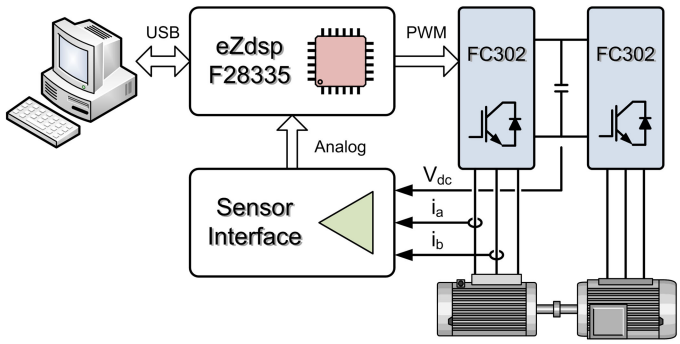

Fig. 5. Experimental setup of the sensorless PMSM drive.

In practice, the two parameter estimators are enabled for distinct speed ranges: the stator resistance estimator is active at low speeds, where the voltage drop on R_s prevails, and the flux estimator is active at high speeds, where the EMF is large.

The stability proof for R_s estimation is based on the fact that the current observer (7), (8) and the parameter observer $\hat{R}_s$ (27) are frequency separated. The current observer has very small time constant $L_{dq}/(R_{s0} + K_{dq}) = 0.5$ ms, and the resistance observer has a convergence rate of several seconds (3 s in Fig. 10). For steady-state operation, the $\hat{i}_y$ current is proportional with the conductance $\hat{G}_s = 1/\hat{R}_s$. It follows that the transfer function from the actual i_y to $\hat{G}_s$ is a first-order low-pass filter, which is stable for any positive K_{Rs}.

VI. Experimental Results

The experimental drive setup consists of a 0.5-kW PMSM connected to an induction machine (IM) used for loading. The PMSM has a rotor with surface-mounted magnets, and its nominal data and parameters are $U_N = 400$ V, $n_N = 1500$ r/min, $f_N = 50$ Hz, $T_N = 3$ N·m, $L_d = 98$ mH, $L_q = 94$ mH, $R_s = 16\,\Omega$ (cold state), $\lambda_{\rm PM} = 0.9$ Wb, $p = 2$, and $J = 0.005$ kg·m^2. This motor has a large cogging torque, with peaks up to 0.5 N·m (0.17 p.u.), which acts as a variable-load perturbation. Low-frequency torque oscillations visible in all experiments are due to this torque. Both machines are supplied by Danfoss FC302 open-architecture inverters connected by a common dc link and controlled by two eZdsp-F28335 DSP cards from Texas Instruments. The sampling-time and PWM frequency is $f_s = 10$ kHz, and the code is written in C++. Two currents and the dc voltage are measured, and an encoder with 5000 lines is used for speed monitoring. Fig. 5 shows a simplified schematic of the PMSM drive experimental setup.

This drive uses a conventional field-oriented control system that employs PI current controllers in a synchronous frame, with constant d-current reference $i_d^* = 0.5$ A. Other controllers, like direct torque controller, can also be used [27]. The speed controller is a simple PI that produces the q^*-current reference. The observer gains for all experiments are $K_d = K_q = 300$ V/A for a bandwidth of 500 Hz, $k_\theta = 200$ rad/s·A^{-1}, $K_\omega = -80\,000$ rad/s^2·A^{-1}, $K_T = 8000$

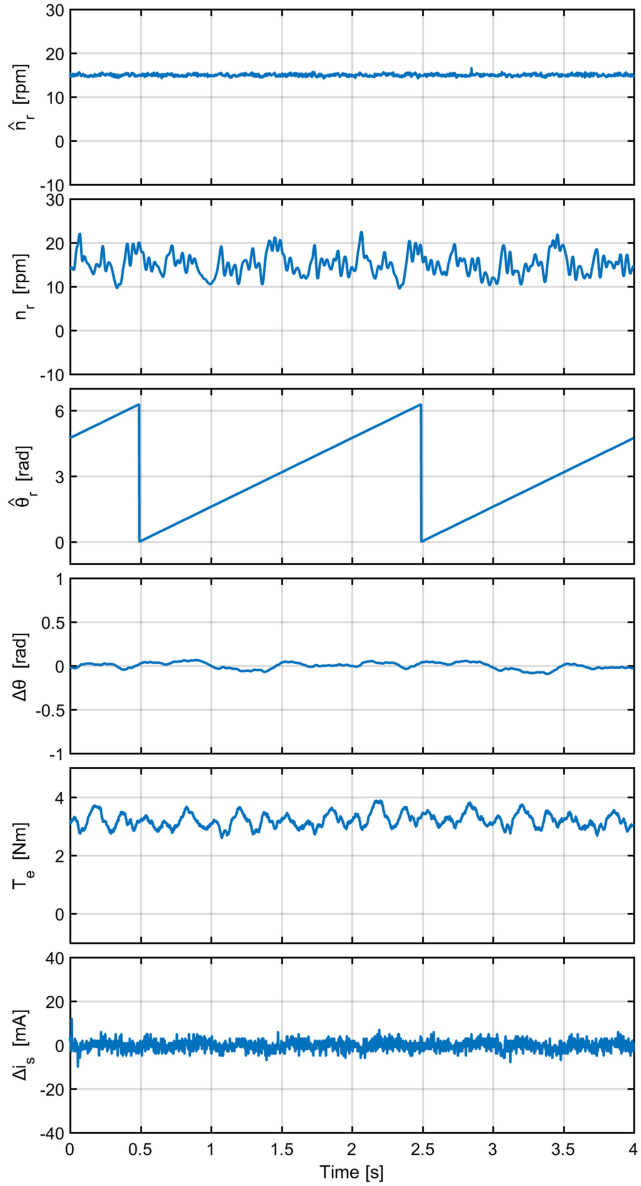

Fig. 6. Low-speed steady-state operation at 15 r/min (0.5 Hz) and 3-N·m load.

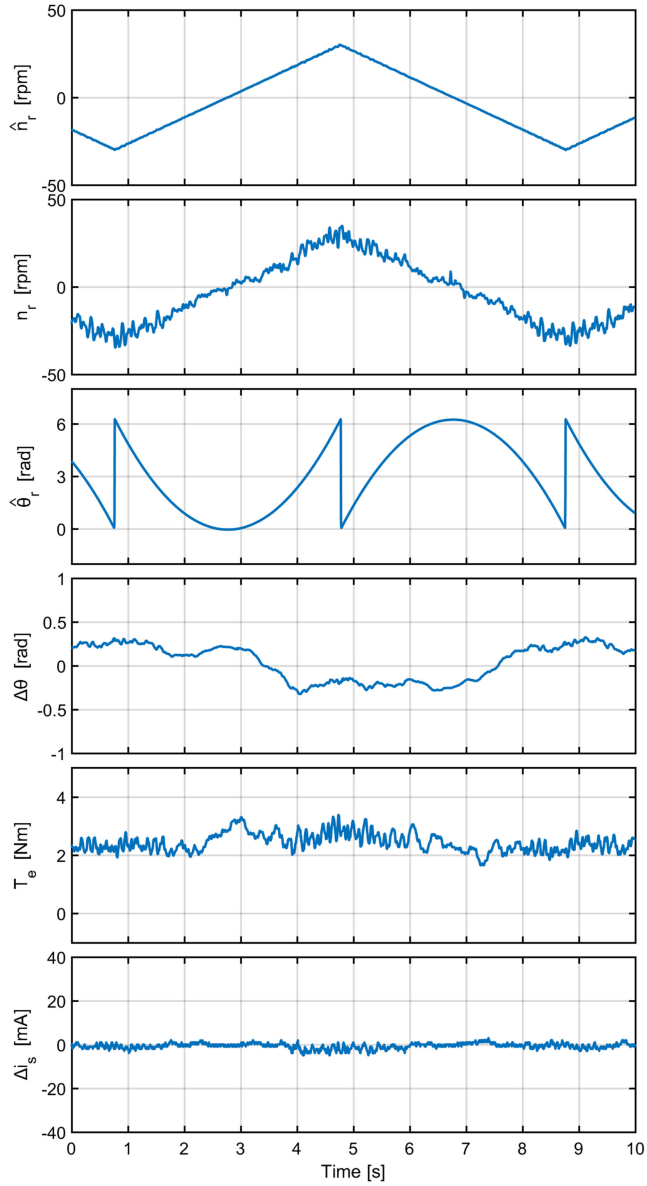

Fig. 7. Slow-speed reversals between ±30 r/min, with rated load.

N·m/s·A^{-1}, and $K_{Rs} = 10$ Ω/s·A^2. Most of the experiments have been focused on low-speed operation.

A. Low-Speed Operation

Fig. 6 shows the steady-state operation at 15 r/min (1% rated speed and 0.5-Hz stator frequency) with a rated load of 3 N·m. From top to bottom, the waveforms are estimated rotor speed $\hat{n}_r$, measured speed n_r, estimated electrical rotor position $\hat{\theta}_r$, position estimation error $\Delta\theta$, estimated electromagnetic torque T_e, and current magnitude estimation error $\Delta i_s = |i_s| - |\hat{i}_s|$. It is notable that the estimated current matches very well with the real current, which proves the observer accuracy. The position estimation error is less than ±0.1 rad (5.7°), while the speed error is within ±5 r/min. Despite the large load pulsations, the machine torque T_e also tracks well the load torque T_L.

Motor and generator operation at low speeds, during speed transients, is demonstrated in Figs. 7 and 8. Fig. 7 shows slow-speed reversals between ±30 r/min, with ramps of 15 r/min/s. Fig. 8 shows fast (step) speed reversals between ±15 r/min with a 4-s period. The same waveforms as in Fig. 6 are displayed. The estimated current errors are very small, which is an indication of the observer accuracy at very low speeds.

It is notable that the observer remains stable at and near zero speed crossings during slow reversals; however, the position error increases significantly in this region. The instability at zero speed, which is inherent to all observers that use the fundamental excitation, occurs after several seconds of operation near zero speed with load torque.

A performance comparison of the proposed PLL observer versus three recent observers, the reduced-order adaptive observer [8], the extended EMF observer [29], and the extended

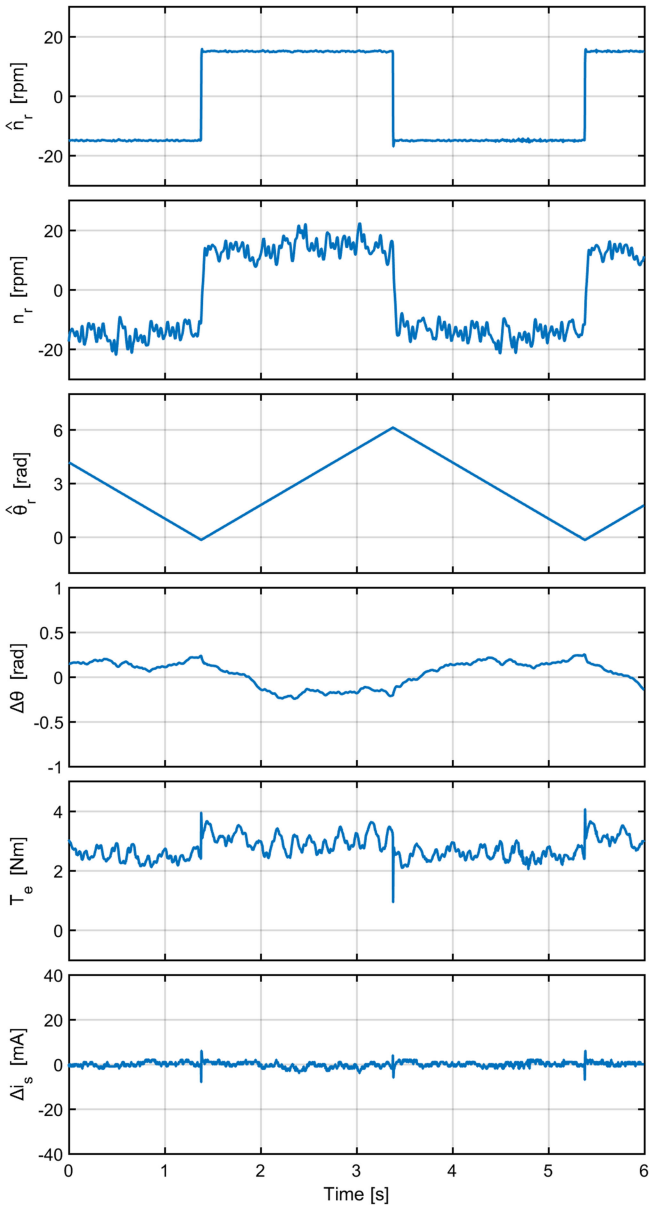

Fig. 8. Fast-speed reversals between ±15 r/min, with rated load.

TABLE I
COMPARISON OF OBSERVER ACCURACY AT LOW SPEEDS

Obs. Type	Min speed [rpm] with rated torque	Δθ [deg]	Δn [rpm]	Bandwidth [Hz]	R_s estimation
[8]	30 (0.02 pu)	±3	± 14	n/a	yes
[29]	170 (0.08 pu)	-7; 14	n/a	4	no
[30]	50 (0.033 pu)	-15; 9	± 12	n/a	no
PLL	15 (0.01 pu)	±5	± 5	12	yes

flux model observer [30], is presented in Table I. This comparison considers the lowest effective (reported) speed with rated load, the position and speed estimation accuracy, the observer bandwidth, and the R_s estimation.

The proposed observer allows operating at the lowest speed and works with the smallest speed errors. This article and [8] provide parameter sensitivity analyses and real-time identification of the stator resistance and PM flux, essential for stable and accurate low-speed operation. Motoring and generating operation with fast and slow reversals is also demonstrated in [8] and in this article.

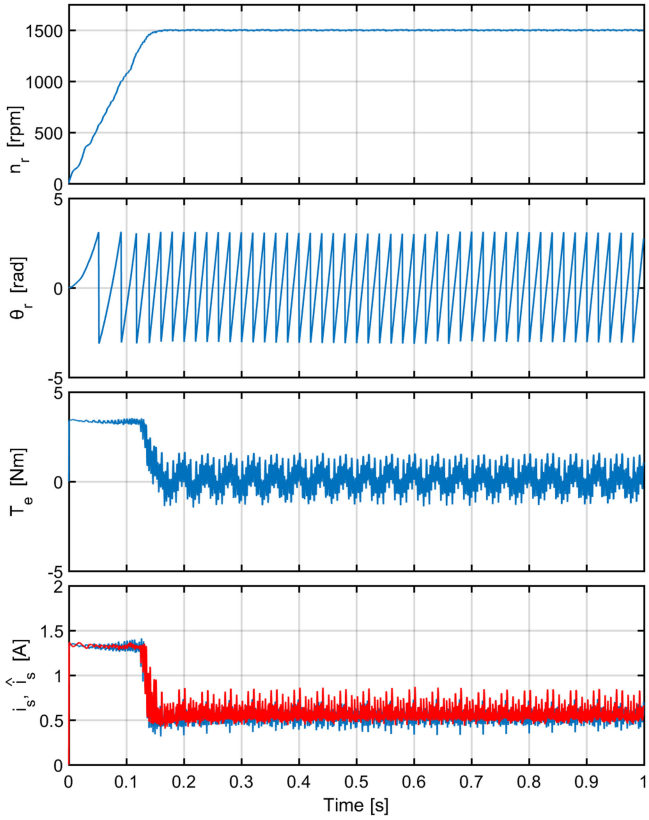

Fig. 9. Startup from 0 to 1500 r/min with step speed reference.

B. High-Speed Operation

Drive startup from zero to rated speed and high-speed operation are illustrated in Fig. 9. The waveforms are: rotor speed n_r, rotor position θ_r, estimated torque T_e, measured and estimated current magnitudes, $|i_s|$ and $|i_s|$. During the acceleration, the torque reference is limited to rated torque $T^*_{e\,\max} = 3$ N·m by the speed controller. It is notable that the current observer is not much affected by the large speed and torque transients that occur during startup. For steady-state operation, i_d and i_q current errors are somewhat larger than those for low speeds, but overall these errors remain small in all situations.

C. Stator Resistance Estimation

Stator resistance estimation is demonstrated in Fig. 10 for operation 60 r/min (2-Hz stator frequency) with 2.5-N·m load torque. The waveforms are estimated resistance $\hat{R}_s$, estimated rotor speed $\hat{n}_r$, and estimated torque T_e. Initial resistance is $R_{s0} = 15\ \Omega$, the estimation starts at 0.8 s, and the resistance reaches almost 18 Ω after 4 s. This value includes the actual stator resistance and the equivalent ON-state resistance of the IGBTs and diodes. For this test only, the estimation gain is

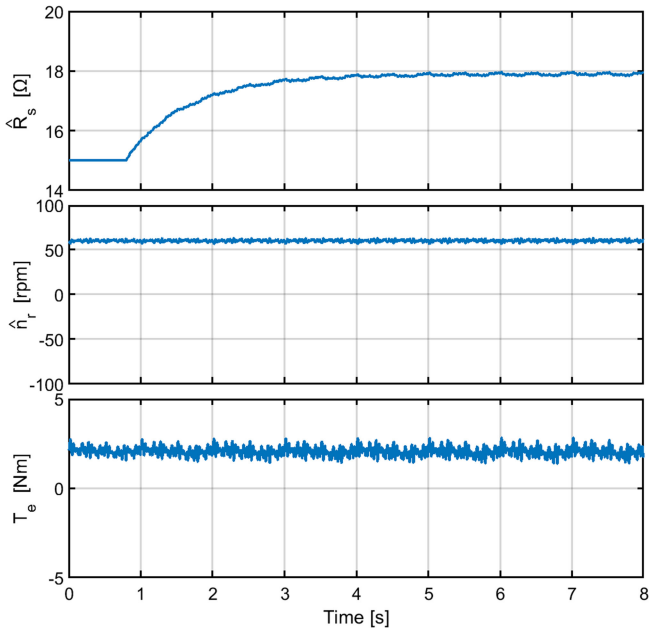

Fig. 10. Stator resistance estimation for steady-state operation at 60 r/min (2-Hz stator frequency) with 2.5-N·m load torque.

large as $K_{Rs} = 400$ to better illustrate the convergence over a short time interval. We obtained identical results for operation at negative speeds. It was experimentally determined that the resistance adaptation increases the robustness at all speeds, and it is critical for low-speed operation.

VII. Conclusion

In this article, a new PLL state observer topology with an integrated decoupled stator current observer for sensorless control of PMSM drives, for wide-speed-range operation, was proposed. The original contributions of this article were as follows.

1) Key dependences between the stator current errors and the rotor position and speed errors were established. Unlike existing solutions, the current errors were obtained as outputs of a closed-loop (true) observer, not as differences between the real and estimated models.
2) A new observer topology was proposed. It contained two interconnected observers with independent corrections: a) a second-order PLL observer that estimates the rotor position using the direct current error as a phase error correction and b) a third-order extended Luenberger observer that estimates the rotor speed using the quadrature current error as the correction term. This scheme did not use stator flux observers, which employed the voltage integrator with well-known disadvantages, or other equivalent integrators that failed at low speeds.
3) To improve the position estimation accuracy, a real-time stator resistance estimator for low-speed operation and a PM flux estimator for high-speed operation were proposed, based on the fact that the quadrature current was zero in the current reference frame.
4) Experimental results prove the effectiveness, static and dynamic performance, and robustness of the new observer with stator resistance estimation for wide-speed-range operation. The minimum speed in motoring and generating modes was less than 15 r/min (1% of rated speed) with rated load torque, including ramp and step speed reversals.

References

[1] S.-K. Sul, Y.-C. Kwon, and Y. Lee, "Sensorless control of IPMSM for last 10 years and next 5 years," *CES Trans. Elect. Mach. Syst.*, vol. 1, no. 2, pp. 91–99, Jun. 2017.
[2] D. Xu, B. Wang, G. Zhang, G. Wang, and Y. Yu, "A review of sensorless control methods for AC motor drives," *CES Trans. Elect. Mach. Syst.*, vol. 2, no. 1, pp. 104–115, Mar. 2018.
[3] S. Morimoto, M. Sanada, and Y. Takeda, "Mechanical sensorless drives of IPMSM with online parameter identification," *IEEE Trans. Ind. Appl.*, vol. 42, no. 5, pp. 1241–1248, Sep./Oct. 2006.
[4] Z. Chen, M. Tomita, S. Doki, and S. Okuma, "An extended electromotive force model for sensorless control of IPMSM," *IEEE Trans. Ind. Electron.*, vol. 50, no. 2, pp. 288–295, Apr. 2003.
[5] Z. Qiao, T. Shi, Y. Wang, Y. Yan, C. Xia, and X. He, "New sliding-mode observer for position sensorless control of PMSM," *IEEE Trans. Ind. Electron.*, vol. 60, no. 2, pp. 710–719, Feb. 2013.
[6] A. Piipo, M. Hinkkanen, and J. Luomi, "Analysis of an adaptive observer for sensorless control of interior PMSM," *IEEE Trans. Ind. Electron.*, vol. 55, no. 2, pp. 570–576, Feb. 2008.
[7] A. Piipo, M. Hinkkanen, and J. Luomi, "Adaptation of motor parameters in sensorless PMSM drives," *IEEE Trans. Ind. Appl.*, vol. 45, no. 1, pp. 203–212, Jan./Feb. 2009.
[8] M. Hinkkanen, T. Tuovinen, L. Harnefors, and J. Luomi, "A combined position and stator-resistance observer for salient PMSM drives: Design and stability analysis," *IEEE Trans. Power Electron.*, vol. 27, no. 2, pp. 601–609, Feb. 2012.
[9] N. Matsui, "Sensorless PM brushless DC motor drives," *IEEE Trans. Ind. Electron.*, vol. 43, no. 2, pp. 300–308, Apr. 1996.
[10] Y. Lee and S.-K. Sul, "Model-based sensorless control of an IPMSM with enhanced robustness against load disturbances based on position and speed estimator using a speed error," *IEEE Trans. Ind. Appl.*, vol. 54, no. 2, pp. 1448–1459, Mar./Apr. 2018.
[11] M. Eskola and H. Tuusa, "Comparison of MRAS and novel simple method for position estimation in PMSM drives," in *Proc. IEEE 34th Ann. Conf. Power Electron. Spec.*, Jun. 2003, vol. 2, pp. 550–555.
[12] S. Koonlaboon and S. Sangwongwanich, "Sensorless control of interior permanent magnet synchronous motors based on a fictitious permanent magnet flux model," in *Proc. 40th IEEE Ind. Appl. Soc. Annu. Meeting*, Oct. 2005, pp. 311–318.
[13] I. Boldea, M. C. Paicu, and G. D. Andreescu, "Active flux concept for motion-sensorless unified AC drives," *IEEE Trans. Power Electron.*, vol. 23, no. 5, pp. 2612–2618, Sep. 2008.
[14] M. H. Bierhoff, "A general PLL-type algorithm for speed sensorless control of electrical drives," *IEEE Trans. Ind. Electron.*, vol. 64, no. 12, pp. 9253–9260, Dec. 2017.
[15] M. Abdelrahem, C. M. Hackl, and R. Kennel, "Finite position set-phase locked loop for sensorless control of direct-driven permanent-magnet synchronous generators," *IEEE Trans. Power Electron.*, vol. 33, no. 4, pp. 3097–3105, Apr. 2018.
[16] M. Fatu, C. Lascu, G. D. Andreescu, R. Teodorescu, F. Blaabjerg, and I. Boldea, "Voltage sags ride-trough of motion sensorless controlled PMSG for wind turbines," in *Proc. 42nd IEEE Ind. Appl. Soc. Annu. Meeting*, Sep. 2007, vol. 1, pp. 171–178.
[17] S.-C. Yang and R. D. Lorenz, "Surface permanent-magnet machine self-sensing at zero and low speeds using improved observer for position, velocity, and disturbance torque estimation," *IEEE Trans. Ind. Appl.*, vol. 48, no. 1, pp. 151–160, Jan./Feb. 2012.
[18] P. L. Xu and Z. Q. Zhu, "Carrier signal injection-based sensorless control for permanent-magnet synchronous machine drives considering machine parameter asymmetry," *IEEE Trans. Ind. Electron.*, vol. 63, no. 5, pp. 2813–2824, May 2016.
[19] X. Luo, Q. Tang, A. Shen, and Q. Zhang, "PMSM sensorless control by injecting HF pulsating carrier signal into estimated fixed-frequency rotating reference frame," *IEEE Trans. Ind. Electron.*, vol. 63, no. 4, pp. 2294–2303, Apr. 2016.

[20] P. L. Xu and Z. Q. Zhu, "Novel square-wave signal injection method using zero-sequence voltage for sensorless control of PMSM drives," *IEEE Trans. Ind. Electron.*, vol. 63, no. 12, pp. 7444–7454, Dec. 2016.
[21] C.-E. Hwang, Y. Lee, and S.-K. Sul, "Analysis on position estimation error in position-sensorless operation of IPMSM using pulsating square wave signal injection," *IEEE Trans. Ind. Appl.*, vol. 55, no. 1, pp. 458–470, Jan./Feb. 2019.
[22] G. Wang, D. Xiao, N. Zhao, X. Zhang, W. Wang, and D. Xu, "Low-frequency pulse voltage injection scheme-based sensorless control of IPMSM drives for audible noise reduction," *IEEE Trans. Ind. Electron.*, vol. 64, no. 11, pp. 8415–8426, Nov. 2017.
[23] M. X. Bui, D. Guan, D. Xiao, and M. F. Rahman, "A modified sensorless control scheme for interior permanent magnet synchronous motor over zero to rated speed range using current derivative measurements," *IEEE Trans. Ind. Electron.*, vol. 66, no. 1, pp. 102–113, Jan. 2019.
[24] C. Silva, G. M. Asher, and M. Sumner, "Hybrid rotor position observer for wide speed-range sensorless PM motor drives including zero speed," *IEEE Trans. Ind. Electron.*, vol. 53, no. 2, pp. 373–378, Apr. 2006.
[25] G. Wang, R. Yang, and D. Xu, "DSP-based control of sensorless IPMSM drives for wide-speed-range operation," *IEEE Trans. Ind. Electron.*, vol. 60, no. 2, pp. 720–727, Feb. 2013.
[26] S. C. Yang and Y. L. Hsu, "Full speed region sensorless drive of permanent-magnet machine combining saliency-based and back-emf-based drive," *IEEE Trans. Ind. Electron.*, vol. 64, no. 2, pp. 1092–1101, Feb. 2017.
[27] C. Lascu, I. Boldea, and F. Blaabjerg, "Super-twisting sliding mode control of torque and flux in permanent magnet synchronous machine drives," in *Proc. 39th Annu. Conf. IEEE Ind. Electron. Soc.*, Nov. 2013, pp. 3171–3176.
[28] D. G. Luenberger, "Observing the state of a linear system," *IEEE Trans. Mil. Electron.*, vol. ME-8, no. 2, pp. 74–80, Apr. 1964.
[29] Y. Lee, Y.-C. Kwon, and S.-K. Sul, "Comparison of rotor position estimation performance in fundamental-model-based sensorless control of PMSM," in *Proc. IEEE Energy Convers. Congr. Expo.*, Sep. 2015, pp. 5624–5633.
[30] Y. Zhao, Z. Zhang, W. Qiao, and L. Wu, "An extended flux model-based rotor position estimator for sensorless control of salient-pole permanent-magnet synchronous machines," *IEEE Trans. Power Electron.*, vol. 30, no. 8, pp. 4412–4422, Aug. 2015.

Cristian Lascu received the B.S., M.Sc., and Ph.D. degrees in electrical engineering from the University Politehnica of Timisoara, Timisoara, Romania, in 1994, 1995, and 2002, respectively.

Since 1995, he has been with the Department of Electrical Engineering, University Politehnica of Timisoara, where he is currently Associate Professor. He was a Visiting Researcher with the Institute of Energy Technology, Aalborg University, Aalborg, Denmark, on several occasions. From 2002 to 2004, he was with SIEI S.p.A, Saronno, Italy, where he was involved in advanced power electronics and drives for electrical vehicles under a European Marie Curie Fellowship. From 2009 to 2011, he was with the Department of Electrical and Biomedical Engineering, University of Nevada Reno, Reno, NV, USA. His current research interests include power electronics and high-performance electrical drives.

Dr. Lascu was a recipient of an IEEE Industry Applications Society Prize Paper Award in 1998.

Gheorghe-Daniel Andreescu (Senior Member, IEEE) was born in Caracal, Romania. He received the M.S. degree in applied electronics and the Ph.D. degree in automatic control systems from the University Politehnica Timisoara (UPT), Timisoara, Romania, in 1977 and 1999, respectively.

Since 1984, he has been with the Department of Automation and Applied Informatics, UPT, where he is currently a Full Professor and Ph.D. Supervisor in Automation (System Engineering). He has authored/coauthored more than 90 papers published in international journals and conference proceedings. He is a reviewer of more than 25 scientific journals indexed in Web of Science. His current research interests include advanced control of ac drives, sensorless control, power electronics control, control of mechatronic systems, and greenhouse climate control systems.

Dr. Andreescu is a Member of the Technical Committee TC4.2 Mechatronics Systems of the International Federation of Automatic Control. He was a recipient of the "Tudor Tanasescu" Award of the Romanian Academy for Advanced Automation in 2016.